Section 6

Developments in global forecast models, case studies, predictability investigations, global ensembles.

Global and Regional EPSs in simulating extremely severe tropical cyclonic storm FANI in a unified modeling framework

Ashu Mamgain, Abhijit Sarkar

National Centre for Medium Range Weather Forecasting (NCMRWF),
Ministry of Earth Sciences, Government of India
A-50, Institutional Area Phase-2, Sector 62, Noida (U.P), India
(ashu.mamgain@gov.in)

The ensemble Prediction system in NCMRWF (called NEPS-G) at 12 km horizontal grid resolution has been running operationally since June 2018 with 22 perturbed members (Mamgain et al 2020a; 2020b). The model features 70 vertical levels ranging from the ground to the model lid at about 80 km above the surface. In the present NEPS-G, the 22 analysis perturbations are generated by Ensemble Transform Kalman Filter (ETKF) method. Perturbations of sea-surface temperature are included in the model perturbations. The model uncertainties are taken care by the Stochastic Kinetic Energy Backscatter (SKEB) and Stochastic Perturbed Tendencies (SPT) schemes. Ten days long forecast provided by NEPS-G at 00 UTC is the combination of 11 members from 00 UTC cycle and lagged 11 members from 12 UTC cycle.

The uncertainty that occurs in the limited area forecasts on both temporal and spatial scales can be represented by EPSs at a regional scale. A Short-range (0-75h) ensemble prediction system (EPS) in the NCMRWF (called NEPS-R; Prasad et al., 2019) is at convective scale (~4km) with 11 perturbed ensemble members. It has 80 vertical levels up to a height of 38.5 km. The model uncertainties are taken care of by Random Parameters (RP) scheme. NEPS-R is centering over the domain 62^{o} E-106^{o} E; 6^{o} S 41^{o} N. To understand the added value of NEPS-R, it is evaluated with respect to the 12-km NEPS-G for an extremely severe tropical cyclonic storm FANI. Day 1 to Day 3 Forecast with 11 perturbed members at 00 UTC from both the models has been considered here for this cyclone case. There is an ongoing study with more number of cyclone cases which will demonstrate the performance of both the models at different stages of cyclone development.

Acknowledgements:
The author would like to thank Julian Heming with the use of MOTCTracker and Helen A. Titley for the use of MOTC post processing methods.

References:

Ashu Mamgain, Abhijit Sarkar, EN Rajagopal (2020a) Medium-Range Global Ensemble **"Medium-range global ensemble prediction system at 12 km horizontal resolution and its preliminary validation"**, Meteorological Application, 2020; https://doi.org/10.1002/met.1867

Ashu Mamgain, Abhijit Sarkar, EN Rajagopal (2020b**) "Verification of high resolution (12 km) Global Ensemble Prediction System"**, Atmospheric Research, 2020; https://doi.org/10.1016/j.atmosres.2019.104832

SK Prasad, Abhijit Sarkar and Ashu Mamgain, (2019) **"Implementation of NCMRWF Regional Ensemble Prediction System (NEPS-R)"**, NMRF/TR/09/2019. http://dx.doi.org/10.13140/RG.2.2.26932.94083

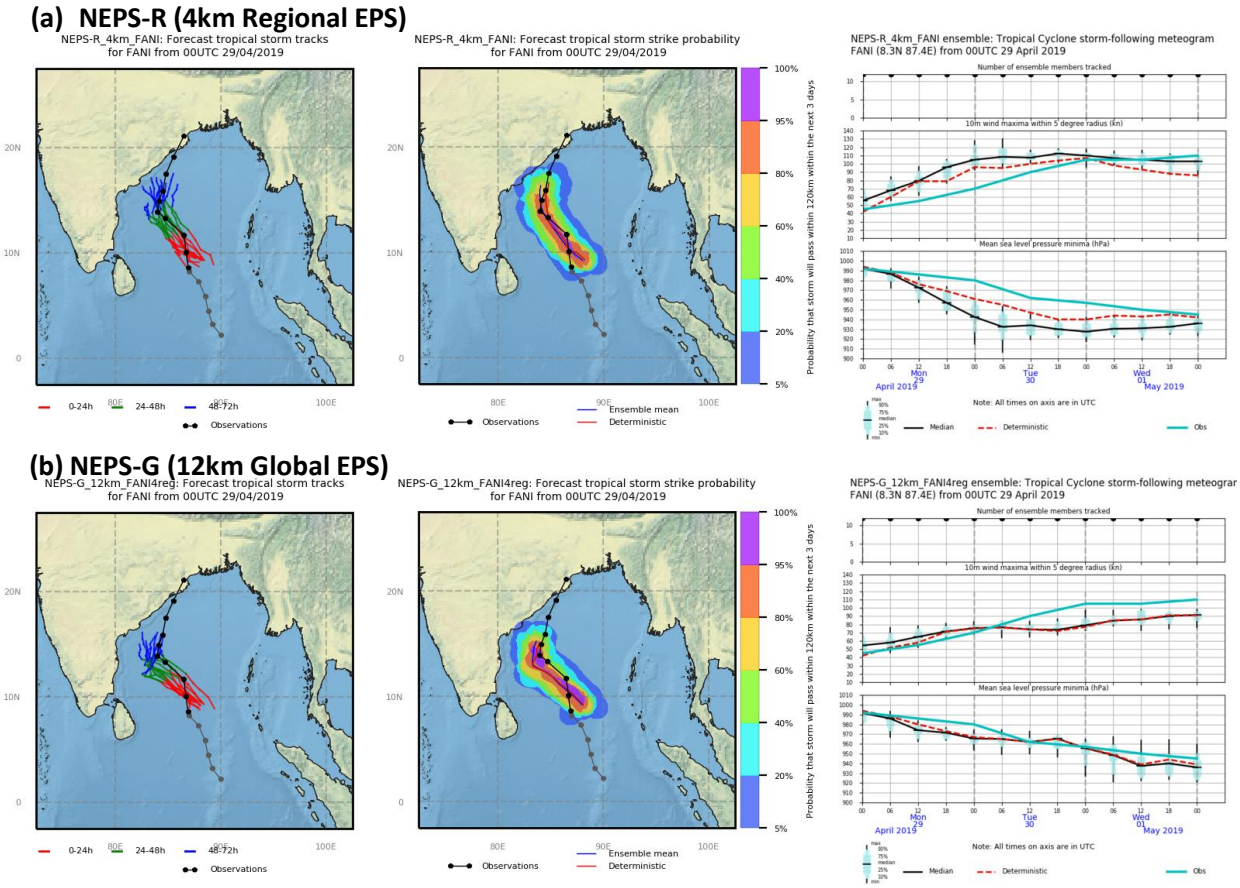

Figure 1. FANI intensified into an extremely severe cyclonic storm and reached its peak intensity on 2nd May 2019. The rapid intensification in wind speed has been nicely captured by NEPS-R as compared to NEPS-G as shown in storm following meteograms. However, NEPS-G performs better in initial stage of cyclone development

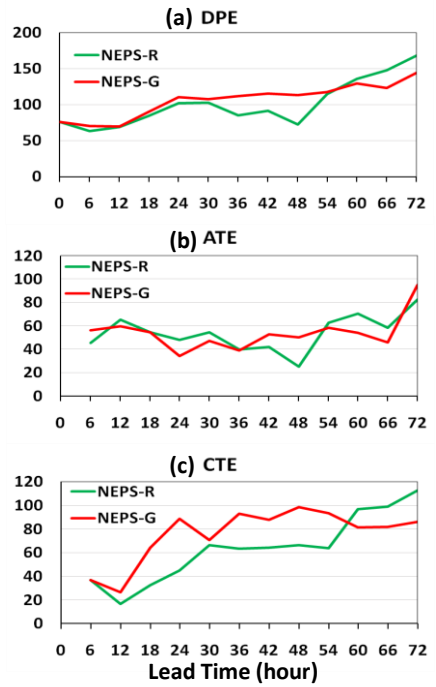

Figure 2. Variation of (a) Direct position error (DPE), (b) Along-track error (ATE), and (c) Cross-track error (CTE) of NEPS-G and NEPS-R with lead time for Fani averaged over 29th April to 2nd May 2019 are shown. DPE and CTE are lower in NEPS-R till 54 hours of the forecast

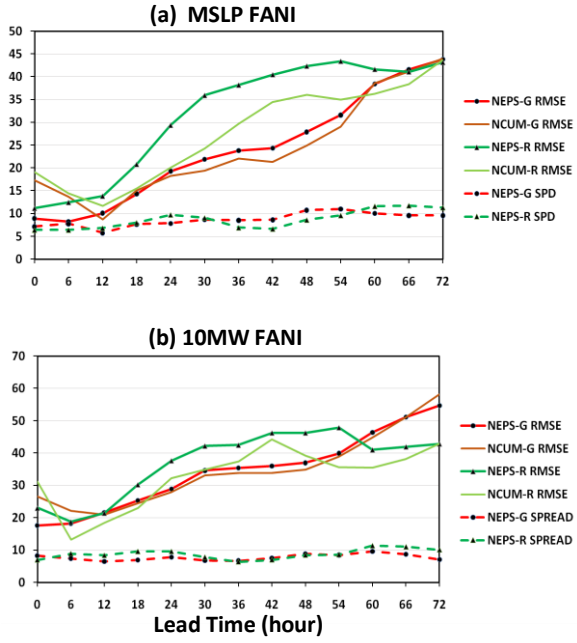

Figure 3. RMSE and Spread in (a) MSLP, and (b) 10m wind speed indicates that RMSE of both the variables are higher in case of NEPS-R whereas spreads in both the models are comparable. NCUM-R is the deterministic/control member of the regional model whereas NCUM-G is deterministic/control member of the global model.

The impact of a high-accuracy high-resolution digital elevation model on numerical weather predictions

Takafumi Kanehama*, Hitoshi Yonehara, Masashi Ujiie
Numerical Prediction Division, Japan Meteorological Agency
*: tkanehama@met.kishou.go.jp

1 Introduction

In numerical weather prediction (NWP), orography is part of the lower-boundary conditions in solving a set of governing equations to determine future atmospheric states. Accurate weather prediction relies on accurate representation of orography in a model, as well as on a model itself, initial states and other boundary conditions. One obvious way to accurately represent orography in a model is to increase horizontal resolutions. Another way is to use accurate source dataset to create orography for target resolutions. In this context, the upgraded Japan Meteorological Agency (JMA) Global Spectral Model (GSM) has been operated since March 2023 [1]. Orography in the upgraded GSM is more accurately represented by increasing both nominal and effective horizontal resolutions and using highly accurate source datasets. This paper describes the effects of high-accuracy high-resolution datasets on numerical weather predictions.

2 GSM Orography

GSM operation involves the use of 1) model mean orography in resolved dynamics, and 2) statistics for subgrid orography representation in orographic drag parameterizations. Both are provided to the model from ancillary files created using source datasets known as digital elevation models (DEMs).

The GSM sources the new MERIT DEM [2] dataset covering the 90°N–60S° region and the new RAMP2 [3] dataset to fill in the 60°S–90°S where MERIT DEM data are unavailable. MERIT DEM is based on Shuttle Radar Topography Mission (SRTM) output [4], representing a quasi-global high-accuracy high-resolution (3 arc-seconds) dataset. Multiple biases in SRTM data are removed in MERIT DEM. In contrast, GTOPO30 [5] was used for the whole globe in the previous version of the GSM [6], which was operated until March 2023.

In the creation of orographic ancillary files, MERIT DEM in 3 arc-seconds is averaged to 30 arc-second grids, which are then combined with RAMP2 data provided in 1-km polar-stereographic form and converted to 30 arc-second lat-lon grids. A model mean orography and statistics for sub-grid orography are created from the resultant global 1-km DEM.

The model mean orography created from the new dataset differs from that of GTOPO30 globally (Figure 1 a). The erroneous mountains in the Guiana Highlands [7] in GTOPO30 are corrected in the new orography. Around Japan, the order of the difference is approximately 10 m. Patchy difference patterns are seen in Figure 1 b, implying that the new model mean orography contains less noise than the previous. This demonstrates that source dataset accuracy influences even coarse-grained fields and a model mean orography, thereby underlining the importance of using a high-accuracy DEM for NWP modeling. Differences are also seen in statistics for subgrid orography between those created from the new and the previous source datasets. The differences in the standard deviation of subgrid orography shown in Figure 2 indicate that those from the new datasets tend to have smoother fields than GTOPO30 data thanks to noise removal (e.g., over Eurasia). However, the standard deviation is larger in new datasets in some regions because the actual resolution in GTOPO30 is coarser than the provided resolution (e.g., over South America).

3 Experiment

The effects of more accurate orography representation and statistics in the GSM were evaluated in data-assimilation experiments for Jan. 2020 and Aug. 2020 against experiments with orography given by GTOPO30. The resolutions were Tq959L128 for 10-day forecasts and 9- and 6-hour forecasts as a first guess, and Tl319L128 for four-dimensional variational assimilation and ensemble forecasts in the data-assimilation cycle.

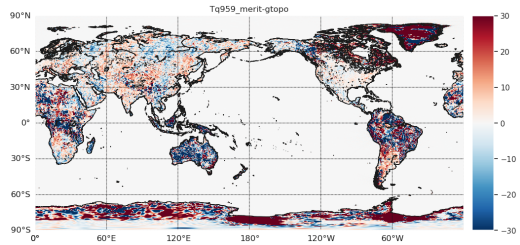

(a)

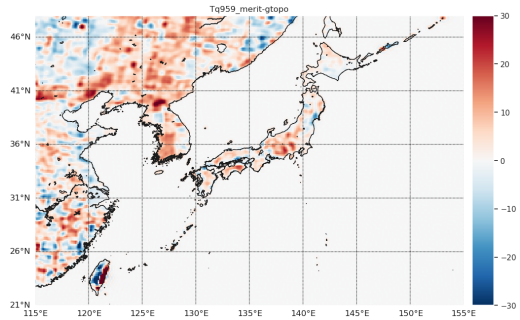

(b)

Figure 1: Differences (MERIT DEM+RAMP2 − GTOPO30) in model mean orography [m] at Tq959: (a) global, and (b) around Japan.

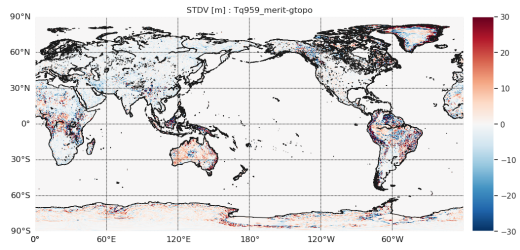

Figure 2: Differences (MERIT DEM+RAMP2 − GTOPO30) in standard deviation of subgrid orography [m] at Tq959.

4 Results

Forecast accuracy was compared in terms of root mean square error (RMSE) against own analysis for geopotential height over the Northern Hemisphere. The RMSE in runs with MERIT DEM+RAMP2 was lower than with GTOPO30 for both winter and summer (Figure 3).

5 Conclusions

Since Mar. 2023, the upgraded JMA GSM has been operated with a model mean orography and statistics for subgrid orography created with the new MERIT DEM and RAMP2 orographic source datasets. The more accurate representation of orography in the GSM contributes to the more accurate analysis and forecasting.

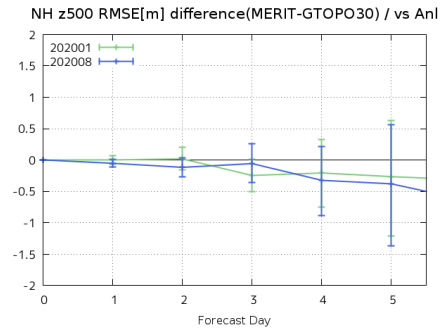

Figure 3: Differences in root mean square error (RMSE) [m] for geopotential height fields over the Northern Hemisphere between experiments with MERIT DEM+RAMP2 and GTOPO30 orography up to 5-day forecasts. Error bars indicate 95% statistical significance estimated using the bootstrap method.

References

[1] H. Yonehara and coauthors. Upgrade of JMA's Operational Global Numerical Weather Prediction System. *Research activities in Earth system modelling*, Vol. 53, , 2023.

[2] D. Yamazaki and coauthors. A high-accuracy map of global terrain elevations. *Geophysical Research Letters*, Vol. 44, No. 11, pp. 5844–5853, 2017.

[3] H. Liu and coauthors. *Radarsat Antarctic Mapping Project Digital Elevation Model, Version 2*. NASA National Snow and Ice Data Center Distributed Active Archive Center, 2015.

[4] T. G. Farr and coauthors. The shuttle radar topography mission. *Reviews of geophysics*, Vol. 45, No. 2, 2007.

[5] D. B. Gesch and coauthors. New land surface digital elevation model covers the Earth. *Eos Trans. AGU*, Vol. 80, No. 6, p. 69, 1999.

[6] Japan Meteorological Agency. *Outline of Operational Numerical Weather Prediction at JMA*. Japan Meteorological Agency, 2021.

[7] K. Iwao and coauthors. Validating global digital elevation models with degree confluence project information and ASTER-DEM on geo grid. *Int. Arch. Photogramm, Remote Sens and Spatial Info. Sci*, Vol. 37, pp. 1847–1852, 2008.

Development of a High-Resolution Global Forecast System Model with a Triangular Cubic Octahedral Grid

Siddharth Kumar[1], Prajeesh A.G. [2], R. Phani[1], Kumar Roy[3], Malay Ganai[1], Tanmoy Goswami[1], P. Mukhopadhyay[1*]

1 Indian Institute of Tropical Meteorology, Ministry of Earth Science, Govt. of India, Pune
2 Climate Change Centre, King Abdullah University of Science and Technology, Saudi Arabia
3 University of Victoria, Canada
Email: mpartha@tropmet.res.in

1. Introduction:

The number of small-scale weather extremes has risen exponentially in the past few years. Since the prevalent Global Forecast System (GFS) has an inherent limitation of horizontal resolution, a dire need was felt to have a forecast model capable of providing increased horizontal resolution to forecast extreme weather events much ahead of time. However, directly increasing the resolution poses computational and other challenges. Hence to overcome these issues in the existing model, a new reduced Gaussian grid called Triangular Cubic Octahedral (TCO) grid was adopted (following Malardel, Sylvie, et al. "A new grid for the IFS." ECMWF newsletter 146.23-28 (2016): 321.). In the original reduced Gaussian Grid, the number of longitude points per latitude remains fixed in different blocks of latitudes, whereas in the TCO Grid, the latitude circle closest to the pole consists of 20 longitude points, and the number of longitude points increases by four at each latitude circle, moving from poles towards the equator. Moreover, unlike the original-reduced Gaussian Grid, the number of longitude points in the TCO grid jumps from one latitude circle to the other by a constant number. Therefore, the horizontal resolution varies smoothly with latitudes. This configuration is obtained by the projection of a sphere on an octahedron. The TCO grid provides a horizontal resolution of near 6kms in the tropics which gives a much finer resolution than the near 12kms of the GFS.

The TCO grid uses cubic truncation in which each wave is represented by four grid points instead of two - as in the linear truncation of GFS.Using a TCO grid over a conventional reduced Gaussian Grid has various advantages. To name a few:

a. Orography is represented in a better way
b. Conservation of mass, momentum, and energy is well-captured
c. Computation of local derivatives is more efficient
d. Model is more scalable
e. Less diffusion is needed to reduce noise.

While the 12 km GFS model helps generate block-level forecasts, IITM's High-Resolution Global Forecast Model (HGFM) model will help reach forecasts on a spatial scale smaller than a block level. Currently, the development of the model is being accomplished by following steps:

i. A basic version of the model involving only the dynamical core is developed first.
ii. All the necessary input files are prepared on the new TCO grid
iii. Individual pieces like dynamical core, necessary input files and model physics are put together to build the full fledge model completely indigenously.
iv. Numerical diffusion is modified

2. Preliminary Results:

The HGFM model (GFS TCO) considerably improves the probability density function of rain over Indian landmass as depicted in Fig. 1. In a case study of an extreme rain event on 22nd August 2022; the HGFM model outperformed the existing GFS model (Fig. 2)

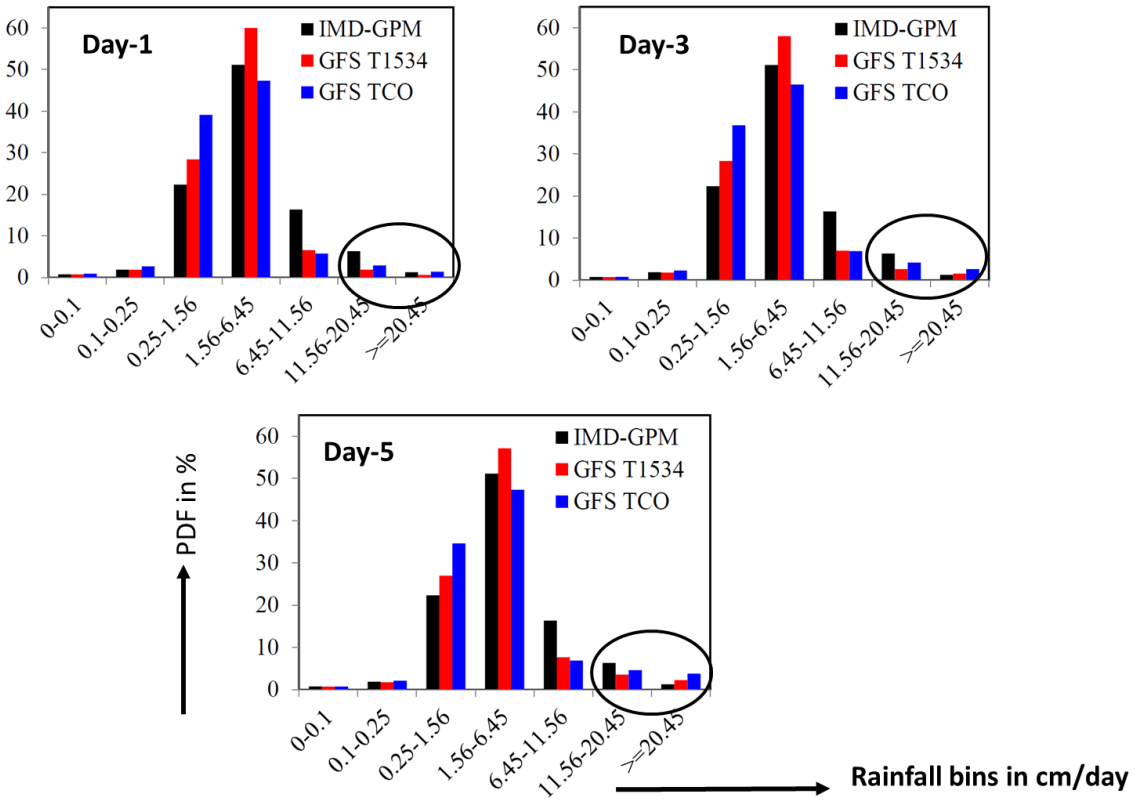

Fig. 1. Rainfall PDF (%) over ALL India landmass

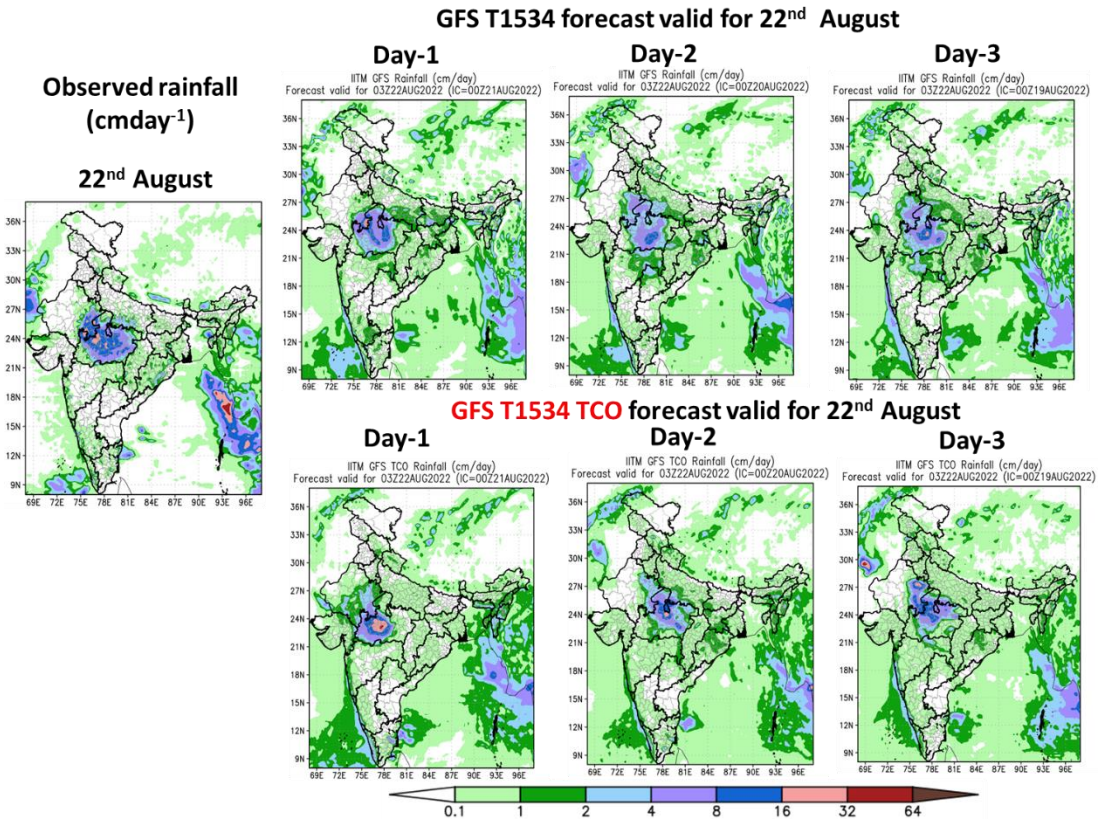

Fig. 2. Extreme rainfall event on 22nd August 2022

Predictability of climate anomalies in the North Eurasian regions during the spring-summer months in relation to El Niño: A case study for 2023

Mokhov I.I.
A.M. Obukhov Institute of Atmospheric Physics RAS
Lomonosov Moscow State University
mokhov@ifaran.ru

Possible anomalies of surface air temperature and precipitation in the Russian regions in the spring-summer months of 2023 are estimated similarly to [1–6] using long-term regional seasonal data and taking into account the La Niña phase (*L*-phase) at the beginning of the year. Also, the results of forecast model calculations made by May 2023 [7] were taken into account. According to ensemble model calculations, the probability of transition to the *E*-phase by the end of 2023 (*L*→*E* transition) is expected to be more than 90%. The corresponding probability for the neutral *N*-phase (*L*→*N* transition) is estimated to be less than 10%, and the probability for the *L*-phase (*L*→*L* transition) is even lower. It is worth to note, that according to [8], the frequency of *L*→*E* and *L*→*L* transitions has been decreasing in recent decades.

Surface temperatures δ*T* and precipitation δ*P* are analyzed for the European (ER) and Asian (AR) regions of Russia at mid-latitudes based on observations since 1891 [9]. To assess the effects of El Niño/La Niña, their indices were used, characterized by the sea surface temperature in the regions of Niño3 and Niño4 in the equatorial latitudes of the Pacific Ocean.

Table 1. Probability of positive and negative surface air temperature anomalies (δ*T*) in the ER (and AR) in May-June-July for different transitions from La-Nina conditions at the beginning of the year (characterized by indices Nino3 and Nino4) from observations since 1891 (n – number of years).

δ*T*, K ER (AR)		>0				≤0			
		> 0		> 1 K		≤ 0		< -1 K	
Nino3 *n*=29	***L→E*** *n*=7	0.41 (0.62)	0.57 (0.71)	0.17 (0.21)	0.29 (0.14)	0.59 (0.38)	0.43 (0.29)	0.14 (0.10)	0.29 (0.29)
	L→N *n*=13		0.38 (0.62)		0.15 (0.23)		0.62 (0.38)		0.15 (0.08)
	L→L *n*=9		0.33 (0.56)		0.11 (0.22)		0.67 (0.44)		0 (0)
Nino4 *n*=28	***L→E*** *n*=4	0.43 (0.54)	0.50 (0.50)	0.21 (0.25)	0.25 (0.25)	0.57 (0.46)	0.50 (0.50)	0.07 (0.07)	0 (0.25)
	L→N *n*=14		0.43 (0.57)		0.21 (0.29)		0.57 (0.43)		0.07 (0.07)
	L→L *n*=10		0.40 (0.50)		0.20 (0.20)		0.60 (0.50)		0.10 (0)

Table 1 shows estimates of the probability of temperature anomalies δ*T* in ER and AR in May-June-July for various transitions from the *L*-phase at the beginning of the year using different El Niño indices. According to these estimates, for the most probable *L*→*E* transition in 2023 with the formation of the canonical El Niño, characterized by the Niño3 index, positive temperature anomalies in the ER and AR are more likely. At the same time, extreme positive temperature anomalies (> 1 K) were estimated as more probable in ER than in AR. With the development of El Niño, revealed by positive anomalies of the Niño4 index, for the *L*→*E* transition, positive and negative temperature anomalies in ER and AR in May-June-July are equally probable.

Corresponding estimates of the probability of precipitation anomalies δP in ER and AR in May-June-July for various transitions from the L-phase at the beginning of the year using various El Niño indices are presented in Table 2. According to these estimates, for the most probable *L*→*E* transition in 2023 with the formation of the canonical El Niño, characterized by the Niño index3, negative and extreme (< -20%) negative precipitation anomalies are more likely in AR and less likely in ER. With the development of El Niño, revealed by positive anomalies of the Niño index4, for the *L*→*E* transition in May-June-July, negative and positive anomalies in precipitation are equally likely for the ER, and negative anomalies are more likely

for the AR. At the same time, extreme (< -20%) negative precipitation anomalies are equally likely in AR and EP.

Table 2. Probability of positive and negative surface air temperature anomalies (δ*P*) in the ER (AR) in May-June-July for different transitions from La-Nina conditions at the beginning of the year (characterized by indices Nino3 and Nino4) from observations since 1891 (n – number of years).

δ*P*, % ER (AR)		<0				≥0			
		<0		< -20%		≥0		>20%	
Nino3	***L→E*** *n*=7	0.41 (0.45)	0.43 (0.57)	0.10 (0.14)	0.14 (0.29)	0.59 (0.55)	0.57 (0.43)	0.14 (0.10)	0 (0.14)
	L→N *n*=13		0.31 (0.31)		0 (0.08)		0.69 (0.69)		0.08 (0.15)
	L→L *n*=9		0.56 (0.56)		0.22 (0.11)		0.44 (0.44)		0 (0)
Nino4	***L→E*** *n*=4	0.50 (0.46)	0.50 (0.75)	0.11 (0.14)	0.25 (0.25)	0.50 (0.54)	0.50 (0.25)	0.04 (0.04)	0 (0)
	L→N *n*=14		0.43 (0.36)		0.21 (0.29)		0.57 (0.64)		0.07 (0.07)
	L→L *n*=10		0.60 (0.50)		0.20 (0.20)		0.40 (0.50)		0 (0)

The formation of noted seasonal anomalies is facilitated by atmospheric blockings against the background of a tendency for a regional decrease in precipitation, which accompanies an increase of surface air temperature. According to ensemble model estimates under warming in the 21st century an increase in the frequency of atmospheric blockings in the regions of the Northern Hemisphere is expected [10]. In [11] the regional features of summer atmospheric blockings in the Northern Hemisphere were noted for different El Niño phase transitions, taking into account the phases of the Atlantic Multidecadal and Pacific Decadal Oscillations. According to [11], in the years beginning in the La Niña phase, an increase in the frequency of atmospheric blockings over the Russian mid-latitudinal European regions, over the Urals and Western Siberia, and also over the Far East is manifested.

References

[1] Mokhov I.I., Timazhev A.V. (2015) Drought risk in the North Eurasian regions: Assessment of El-Nino effects. *Res. Activ. Atmos. Ocean. Modell.,* E. Astakhova (ed.), WCRP Rep. No. 12/2015, 2, 6–7.

[2] Mokhov I.I., Timazhev A.V. (2016) Weather-climate anomalies in Russian regions: El Niño-associated predictability. *Res. Activ. Atmos. Ocean. Modell*., E. Astakhova (ed.). WCRP Rep. No.15/2016, 6, 9–10.

[3] Mokhov I.I., Timazhev A.V. (2018) Predictability of weather-climate anomalies in the North Eurasian regions during transitions from the La Nina conditions. *Res. Activ. Atmos. Ocean. Modell.,* E. Astakhova (ed.), WCRP Rep. No. 15/2018, 6, 9-10.

[4] Mokhov I.I., Timazhev A.V. (2019) Predictability of weather-climate anomalies in the North Eurasian regions for different ENSO transitions during last decades. *Res. Activ. Atmos. Ocean. Modell.,* E. Astakhova (ed.), WCRP Rep. No. 12/2019, 6, 9-10.

[5] Mokhov I.I., Timazhev A.V. (2020) Climate anomalies in the North Eurasian regions: predictability for different El-Nino conditions. *Res. Activ. Earth System Modell*., E. Astakhova (ed.), WCRP Rep. No. 6/2020, 6, 9-10.

[6] Mokhov I.I. (2021) Predictability of seasonal temperature anomalies in the North Eurasian regions in the La Niña conditions. *Res. Activ. Earth System Modell.,* E. Astakhova (ed.), WCRP Rep. No. 4/2021, 6, 5-6.

[7] https://www.cpc.ncep.noaa.gov/products/analysis_monitoring/lanina/enso_evolution-status-fcsts-web.pdf

[8] Mokhov I.I. (2022) Changes in the frequency of phase transitions of different types of El Nino phenomena in recent decades. *Izvestiya, Atmos. Oceanic Phys.,* **58** (1), 1–6.

[9] Meshcherskaya A.V., Mirvis V.M., Golod M.P. (2011) The drought in 2010 against the background of multiannual changes in aridity in the major grain-producing regions of the European part of Russia. *Tr. MGO,* **563**, 94–121 (in Russian)

[10] Mokhov I.I., Timazhev A.V. (2019) Atmospheric blocking and changes in its frequency in the 21st century calculated with the ensemble of climate models. Russ. Meteorol. Hydrol., **44** (6), 369-377.

[11] Mokhov I.I., Timazhev A.V. (2022) Frequency of summer atmospheric blockings in the Northern Hemisphere in different phases of El Nino and Pacific Decadal and Atlantic Multidecadal Oscillations. *Izvestiya, Atmos. Oceanic Phys.,* **58** (3), 199–207.

Upgrade of JMA's Global Ensemble Prediction System

OTA Yoichiro, CHIBA Jotaro, ICHIKAWA Yuiko, OASHI Hiroaki,
TAKAKURA Toshinari, and YAMAGUCHI Haruki

Japan Meteorological Agency

e-mail: yoichiro-ota@met.kishou.go.jp

1. Introduction

The Japan Meteorological Agency (JMA) upgraded its Global Ensemble Prediction System (Global EPS) on March 14 2023 to incorporate recent Global Spectral Model (GSM) developments and revised sea surface temperature (SST) boundary conditions.

2. Major Updates

(1) Incorporation of recent GSM developments

The forecast model was upgraded to a low-resolution version of the newly revised Global Spectral Model (GSM; Yonehara et al. 2023). Some of the upgrades were already applied in the Global EPS on March 2022 (Yamaguchi et al. 2022) in advance of application to the deterministic high-resolution model.

(2) Revised SST boundary conditions

SST boundary conditions are given via an approach combining SSTs prescribed as persisting anomalies from climatological values and other data operationally precomputed using JMA's atmosphere-ocean coupled Seasonal EPS model (JMA/MRI-CPS3; Hirahara et al. 2023). The area of application for the bias-corrected ensemble mean SST from Seasonal EPS, which was mainly used for the tropics and sub-tropics in the previous system, was expanded to the whole globe to improve temperature prediction for the mid-latitude lower troposphere. The period for which SST is linearly relaxed from climatological extrapolation to the bias-corrected ensemble mean SST from the Seasonal EPS is 6 – 11 days, as in the previous system.

3. Verification Results

To verify system performance for medium-range forecasts with lead times of up to 11 days, retrospective experiments covering periods of three months or more in summer 2021 and winter 2021/22 were conducted. The results showed improved continuous ranked probability score (CRPS) for several elements, including 500 hPa geopotential height (Z500) and 850 hPa temperature (T850) in the extra-tropics. Figure 1 shows CRPSs of Z500 and T850 for the Northern Hemisphere in winter and summer. The RMSE of ensemble mean two-meter temperature (T2m) over the mid-latitude ocean for the summer hemisphere is also improved after lead times of six days when the SST begins to relax toward the seasonal EPS. Figure 2 shows normalized differences of RMSEs for T2m between the new and previous systems. Brier skill scores for precipitation forecasts in Japan were also improved in winter (not shown). Performance for forecasts beyond 11 days was also verified, as reported by Yamaguchi et al. (2023).

References

Hirahara, S., Y. Kubo, T. Yoshida, T. Komori, J. Chiba, T. Takakura, T. Kanehama, R. Sekiguchi, K. Ochi, H. Sugimoto, Y. Adachi, I. Ishikawa, and Y. Fujii, 2023: Japan Meteorological Agency/Meteorological Research Institute-Coupled Prediction System version 3 (JMA/MRI-CPS3). *J. Meteor. Soc. Japan.*, **101**, 149-169, doi:10.2151/jmsj.2023-009.

Yamaguchi, H., Y. Adachi, S. Hirahara, Y. Ichikawa, T. Iwahira, Y. Kuroki, C. Matsukawa, R. Nagasawa, K. Ochi, R. Sekiguchi, T. Takakura, M. Ujiie, and H. Yonehara, 2022: Upgrade of JMA's Global Ensemble Prediction System. *WGNE Res. Activ. Earth Sys. Modell.*, **52**, 6.9-6.10.

Yamaguchi, H., J. Chiba, Y. Ichikawa, and T. Takakura, 2023: Hindcast verification of JMA's GEPS for one-month prediction with a globally expanded two-tiered sea surface temperature approach. *WGNE Res. Activ. Earth Sys. Modell.*, submitted.

Yonehara, H., Y. Kuroki, M. Ujiie, C. Matsukawa, T. Kanehama, R. Nagasawa, K. Ochi, M. Higuchi, Y. Ichikawa, R. Sekiguchi, and S. Hirahara, 2023: Upgrade of JMA's Operational Global Numerical Weather Prediction System. *WGNE Res. Activ. Earth Sys. Modell.*, submitted.

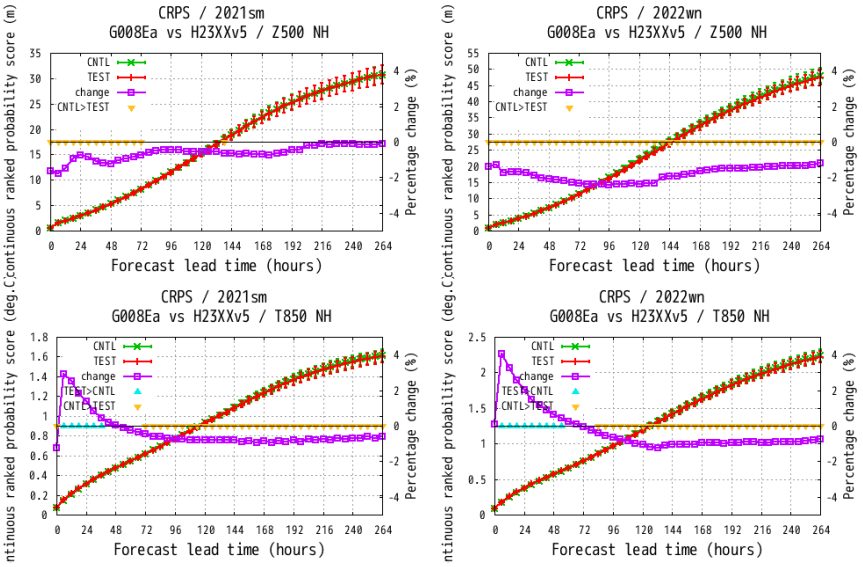

Figure 1: CRPSs of 500 hPa geopotential height (upper; unit: m) and 850 hPa temperature (lower; unit: K) forecasts against analysis for the Northern Hemisphere (20 – 90°N) during 2021 summer (left) and 2021/22 winter (right) as a function of forecast lead times up to 264 hours. The red and green lines represent verification results for the new (TEST) and previous (CNTL) Global EPS (left axis), and the purple line represents ratios of change in scores ([TEST-CNTL]/CNTL, right axis; unit: %). Error bars indicate two-sided 95% confidence levels, and triangles (TEST < CNTL or CNTL < TEST) indicate a statistically significant difference of 0.05.

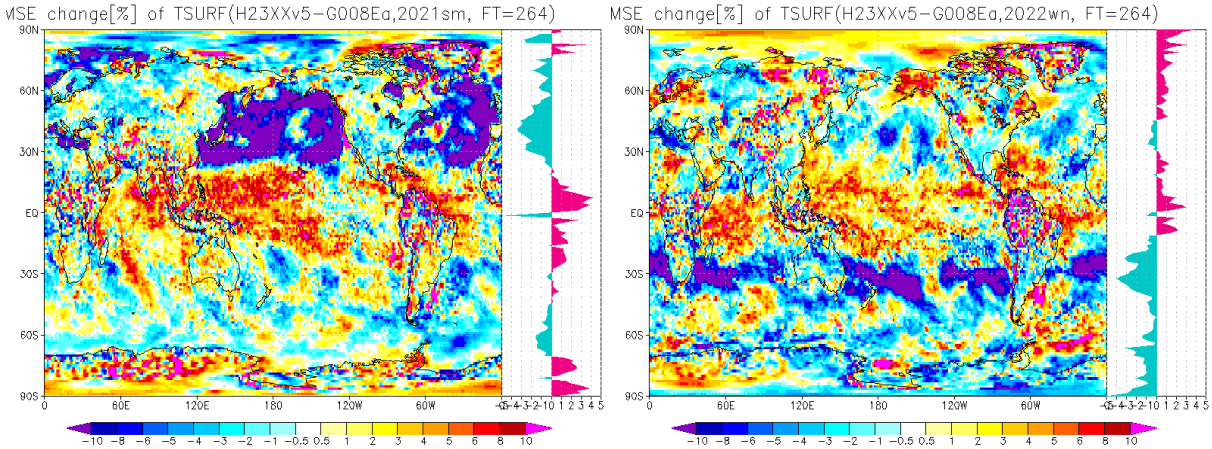

Figure 2: Ratios of change in RMSEs ([TEST-CNTL]/CNTL; unit: %) of two-meter temperature for forecast lead times of 264 hours in summer (left) and winter (right). The graph on the right represents zonal means.

Hindcast verification of JMA's GEPS for one-month prediction with a globally expanded two-tiered sea surface temperature approach

YAMAGUCHI Haruki, CHIBA Jotaro, ICHIKAWA Yuiko, and TAKAKURA Toshinari

Japan Meteorological Agency

e-mail: h.yamaguchi@met.kishou.go.jp

1. Introduction

The Japan Meteorological Agency (JMA) upgraded its Global Ensemble Prediction System (GEPS) on March 14 2023 to incorporate recent Global Spectral Model developments and revised sea surface temperature (SST) boundary conditions (Ota et al. 2023). For the new SST boundary conditions, a two-tiered SST approach (Takakura and Komori 2020) is applied to the whole globe instead of limited areas centered on the tropics and sub-tropics. This paper outlines the results of studies focused on the new SST boundary conditions and the performance of the upgraded GEPS in one-month prediction based on 30-year hindcast experiments.

2. Global Application of the Two-tiered Sea Surface Temperature Approach

In the two-tiered SST approach adopted for the GEPS, SST boundary conditions are prescribed with anomaly-fixed SSTs based on a daily SST analysis (MGDSST; JMA, 2023) at lead times of up to 144 hours, and here are replaced with SSTs derived via bias-corrected ensemble mean forecasts from JMA's Seasonal EPS model (JMA/MRI-CPS3; Hirahara et al. 2023) for lead times of 264 hours or more (with lead times of 144 – 264 hours as relaxation periods). In the previous GEPS, the two-tiered SST approach was applied only to the tropics and sub-tropics because CPS3 SST forecasts exhibit greater levels of error than anomaly-fixed SSTs in the mid-latitudes.

In this study, SSTs were separated into two spatial scales via application of a 1-1-1 filter (a three-point running average) on a 0.25-degree latitude-longitude grid with 30 iterations. The filtered-out spatial variation is referred to as sub-synoptic, and the residual application as synoptic. Sub-synoptic variation included ocean mesoscale eddies in the mid-latitudes. Figure 1 shows that the CPS3-derived SST outperformed the anomaly-fixed SST with respect to synoptic variation but insufficiently represented sub-synoptic variation in the mid-latitudes, partly because the CPS3 ocean model (0.25-degree horizontal resolution) was unable to fully resolve mesoscale eddies. As a result, CPS3-derived SSTs exhibited greater errors than anomaly-fixed SSTs in the mid-latitudes (not shown).

Despite this apparent defect in CPS3-derived SSTs, application of the two-tiered SST approach to the whole globe improved GEPS forecast performance in the mid-latitudes, including improved temperature data for the lower troposphere (especially surface temperature; not shown). Sensitivity experiments clarified that GEPS performance was far more sensitive to synoptic SST variations than to sub-synoptic variations, and the better synoptic variation in the mid-latitudes represented in CPS3-derived SSTs therefore benefited GEPS forecasting skill.

3. Verification Results for the Upgraded GEPS

To verify system performance for one-month forecasts, hindcasts were conducted for 1991 to 2020 for the new GEPS (TEST) and the previous GEPS (CNTL), with use of the latest Japanese reanalysis (JRA-3Q; Kobayashi et al. 2021) for atmospheric initial conditions. The initial dates were the 15th and the end of each month, and the ensemble size was 13 members. Initial perturbations were created from a combination of initial singular vectors (SVs) and evolved SVs, in contrast to the operational system approach (Sekiguchi et al. 2018). Figure 2 shows that the new GEPS was superior to the previous GEPS for surface temperature over oceans in the mid-latitudes, which was consistent with the effects of the new two-tiered SST approach described above.

References

Hirahara, S., Y. Kubo, T. Yoshida, T. Komori, J. Chiba, T. Takakura, T. Kanehama, R. Sekiguchi, K. Ochi, H. Sugimoto, Y. Adachi, I. Ishikawa, Y. Fujii, 2023: Japan Meteorological Agency/Meteorological Research Institute-Coupled Prediction System version 3 (JMA/MRI-CPS3). *J. Meteor. Soc. Japan.*, 101, 149-169, doi:10.2151/jmsj.2023-009.

JMA, 2023: Outline of the operational numerical weather prediction at the Japan Meteorological Agency. Japan Meteorological Agency, Tokyo, Japan.

Kobayashi, S., Y. Kosaka, J. Chiba, T. Tokuhiro, Y. Harada, C. Kobayashi, and H. Naoe, 2021: JRA-3Q: Japanese reanalysis for three quarters of a century. WCRP-WWRP Symposium on Data Assimilation and Reanalysis/ECMWF annual seminar 2021, WMO/WCRP, O4-2, https://symp-bonn2021.sciencesconf.org/data/355900.pdf

Sekiguchi, R., Y. Adachi, T. Kanehama, Y. Kubo, K. Miyaoka, A. Nishimura, A. Shimpo, and T. Yoshida, 2018: Verification of JMA's new GEPS for one-month prediction. *WGNE. Res. Activ. Earth Sys. Modell.*, 48, 6.11-6.12.

Takakura T., and T. Komori, 2020: Two-tiered sea surface temperature approach implemented to JMA's Global Ensemble Prediction System. *WGNE Res. Activ. Earth Sys. Modell.*, 50, 6.15-6.16.

Ota, Y., J. Chiba, Y. Ichikawa, H. Oashi, T. Takakura, and H. Yamaguchi, 2023: Upgrade of JMA's Global Ensemble Prediction System. *WGNE Res. Activ. Earth Sys. Modell.*, submitted.

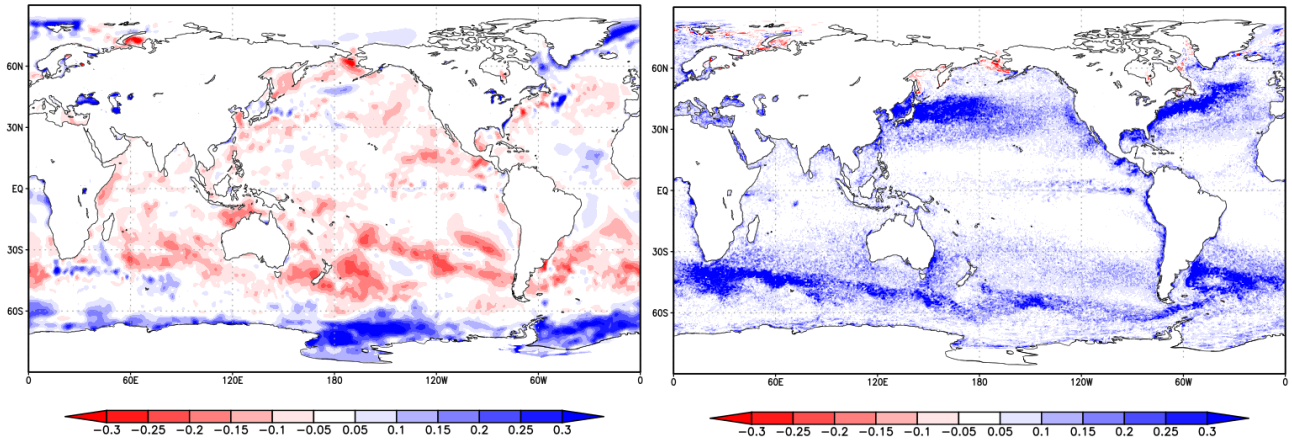

Figure 1: Differences in scale-separated RMSEs between CPS3-derived SSTs and anomaly-fixed SSTs given for forecasts with a 10-day lead time verified against MGDSST. Left: synoptic scale; right: sub-synoptic scale. Negative values indicate smaller CPS3-derived SST errors. Verification period: DJF 2019/2020.

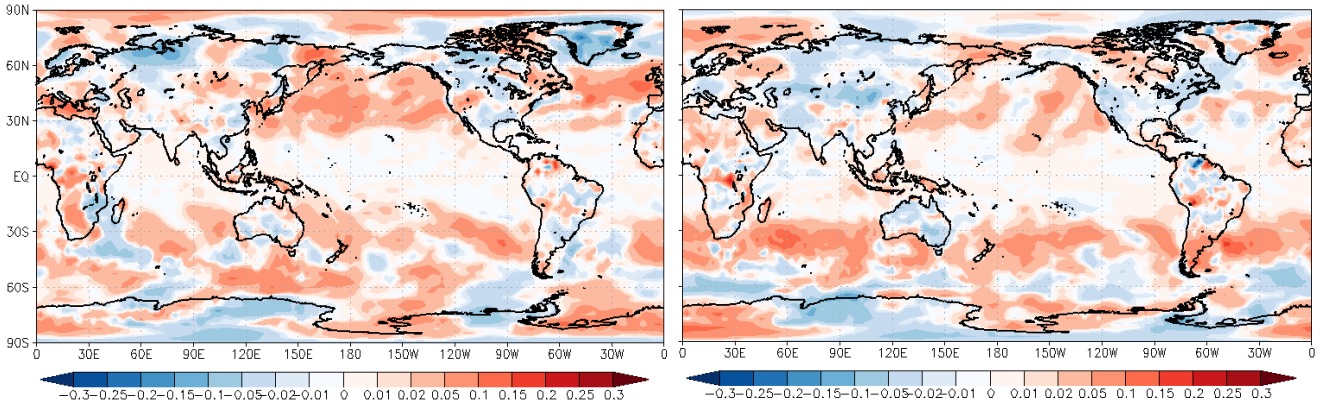

Figure 2: Difference between TEST and CNTL with respect to ensemble-mean anomaly correlation coefficients averaged for initial dates in JJA (left) and DJF (right) over a lead time of the second week (day-10 to 16) for surface temperature verified against JRA-3Q. Positive values: better TEST forecast skill.

Upgrade of JMA's Operational Global Numerical Weather Prediction System

YONEHARA Hitoshi, KUROKI Yukihiro, UJIIE Masashi, MATSUKAWA Chihiro, KANEHAMA Takafumi, NAGASAWA Ryoji, OCHI Kenta, HIGUCHI Mayuko, ICHIKAWA Yuiko, SEKIGUCHI Ryohei, HIRAHARA Shoji
Japan Meteorological Agency, Tokyo, Japan
(email: yonehara@met.kishou.go.jp)

1. Introduction

In March 2023, the Japan Meteorological Agency (JMA) upgraded its operational global Numerical Weather Prediction system (JMA 2023) to incorporate the enhanced horizontal resolution of the JMA Global Spectral Model (GSM). The upgrade also involved refinements such as parametrized surface drag, non-orographic sub-grid gravity waves, and radiation, resulting in better forecasting than the previous versions (Ujiie et al. 2021), particularly in Northern Hemisphere middle latitudes. New source datasets are used for orographic ancillary files (Kanehama et al., 2023). Global snow depth analysis was also improved.

This report outlines individual components of the upgrade and related verification results.

2. Main Updates

2.1 Horizontal resolution

Truncation for spectral dynamics was changed from linear to quadratic to reduce noise on smaller scales with spectral blocking, and grid spacing was enhanced from around 20 km to around 13 km. Effective horizontal resolution was also enhanced by sharpening the model mean topography and weakening fourth-order horizontal spectral numerical diffusion.

2.2 Surface drag

Subgrid-scale orographic drag parameterization (SOD) parameters were revised to reduce stress distribution in the lower stratosphere to improve the weak westerly wind bias in the lower stratosphere. Additionally, the effects of turbulent orographic form drag were strengthened to complement the drag in the mid-lower troposphere weakening due to the SOD revision (Matsukawa et al. 2022).

2.3 Non-orographic gravity wave

In non-orographic gravity wave parameterization, latitudinal dependence of launch momentum flux was improved for reduction at all latitudes, with particularly small fluxes at higher latitudes. This reduced zonal wind and temperature biases in the stratosphere.

2.4 Radiation

The effective size diagnostic scheme for ice clouds in the radiation scheme was changed from that proposed by Wyser (1998) to that of Sun (2001), which applies to tropical and mid-latitude regions. The change resulted in a smaller diagnostic cloud ice effective size and mitigated excess bias in outgoing long-wave radiation flux at the top of the atmosphere due to increased ice cloud optical depth.

Ozone concentration monthly climatology was updated with the 1981–2010 average based on the latest MRI CCM2 reanalysis (Deushi and Shibata 2011) to reduce temperature biases in the stratosphere.

A set of correction schemes for surface downward shortwave radiation (Hogan and Bozzo 2015, Hogan and Hirahara 2016) was incorporated to improve surface radiation fluxes.

2.5 Snow Depth Analysis

The frequency of global snow depth analysis was increased from once a day to four times a day and the analysis method was modified for effective use of satellite snow-cover data.

3 Verification

Two experiments were conducted to compare forecast scores of the previous (CNTL) and updated (TEST) models for July to September 2021 and December 2021 to February 2022. Figure 1 shows root-mean-square error (RMSE) differences for 500-hPa geopotential height forecasts up to 5.5 days ahead verified against own analysis averaged over the Northern Hemisphere (20 – 90°N) for both periods. The upgraded system improved RMSE values of 500-hPa geopotential height and other variables over forecasts of several days as compared to previous GSM versions. The improved accuracy of these forecasts in the troposphere is mainly due to the enhanced accuracy of initial atmospheric conditions resulting from the above improvements in the atmospheric analysis.

References

Japan Meteorological Agency, 2023: Outline of Operational Numerical Weather Prediction at JMA. Japan Meteorological Agency, Tokyo, Japan.

Ujiie, M., M. Higuchi, T. Kadowaki, Y. Kuroki, K. Miyaoka, M, Oda, K. Ochi, R. Sekiguchi, H. Shimizu, S. Yokota, and H Yonehara, 2021: Upgrade of JMA's Operational Global NWP system. WGNE. Res. Activ. Earth. Sys. Modell, 6.9-6.10.

Kanehama, T., H. Yonehara, M. Ujiie, 2023:
The impact of a high-accuracy high-resolution digital elevation model on numerical weather predictions. WGNE. Res. Activ. Earth. Sys. Modell

Matsukawa, C., Y. Kuroki, and T. Kanehama, 2022: Optimization of orographic drag parametrizations in the JMA operational global model using COORDE-type experiments. WGNE. Res. Activ. Earth. Sys. Modell, 4.7-4.8.

Wyser, K., 1998: The Effective Radius in Ice Clouds. J. Climate, 11, 1793-1802.

Sun, Z., 2001: Reply to comments by Greg M. McFarquhar on `Parametrization of effective sizes of cirrus-cloud particles and its verification against observations'. (October B, 1999, 125, 3037-3055). Q. J. R. Meteorol. Soc.,127, 267-271.

Deushi, M. and K. Shibata, 2011: Development of a Meteorological Research Institute chemistry-climate model version 2 for the study of tropospheric and stratospheric chemistry. Pap. Meteor. Geophys., 62, 1–46.

Hogan, R. J. and A. Bozzo, 2015: Mitigating errors in surface temperature forecasts using approximate radiation updates. J. Adv. Model. Earth Syst., 7, 836–853.

Hogan, R. J. and S. Hirahara, 2016: Effect of solar zenith angle specification in models on mean shortwave fluxes and stratospheric temperatures. Geophys. Res. Lett., 43, 482–488.

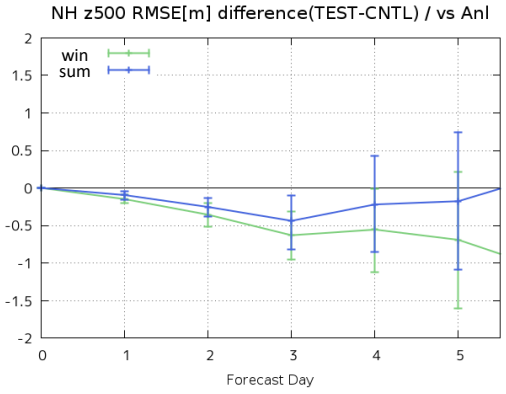

Figure 1. Root-mean-square error differences (TEST – CNTL) of 500-hPa geopotential height [m] against analysis (Anl) in the Northern Hemisphere extra-tropics (20 – 90°N) in the winter and summer experiments. The horizontal axis shows the forecast lead time [days], and the green and blue lines show the winter and summer experiments, respectively. Error bars indicate statistical significance with 95% confidence based on the bootstrap method.